Raman Investigation of Single Oxidized Carbon Nanotubes

ALF MEWS,[a,*] CHAOYANG JIANG,[a] THOMAS SCHUESSLER,[a] GUENTHER PHILIPP,[b] Y. FAN,[b] AND MARKO BURGHARD[b]
[a]Institut für Physikalische Chemie, Universität Mainz, Welderweg 11, 55099 Mainz, Germany
[b]Max-Planck-Institut für Festkörperforschung, Heisenbergstrasse 1, 70569 Stuttgart, Germany

(Received 29 May 2001)

Abstract. The oxidation process of single-walled carbon nanotubes via nitric acid treatment was followed by IR-, UV-Vis-NIR, and single bundle Raman spectroscopy. The introduction of functional, oxygen-containing groups is revealed by an additional absorption band at 1725 cm^{-1}, characteristic of carbonyl stretch vibrations. No significant shift of the optical absorption bands could be detected after oxidation. The combination of atomic force microscopy and confocal scanning resonance-enhanced Raman microscopy was used to investigate thin bundles and, eventually, individual nanotubes in detail. These experiments enabled determination of the dependence of the Raman intensity of the G-line (around 1590 cm^{-1}) on the bundle height for both non-oxidized and oxidized tubes. The Raman cross-section of the oxidized tubes was found to be reduced by a factor of ~4, compared to the pristine tubes. This observation is ascribed to all tubes within a bundle that are oxidized to the same degree.

INTRODUCTION

Single-walled carbon nanotubes (SWCNTs) are molecular wires with high mechanical strength and outstanding electrical properties, which make them excellent components for nanostructured materials such as mechanically reinforced (conductive) composites.[1] For applications along these lines, chemical modification of the nanotubes is of primary importance. In particular, methods have to be developed to render the tubes soluble in organic solvents and to achieve miscibility with different classes of polymer matrices, as well as to introduce functional groups for further chemical processing. During the last 2–3 years, the chemistry of CNTs has been approached mainly on the basis of oxidation[2] and fluorination,[3] in some cases followed by alkyl chain attachment.[4] Nanotube oxidation is a promising first functionalization step since it allows for subsequent modification of the carboxylic functions, for example via formation of amide linkages.[5] However, little is known about the extent of oxidation and its effect on the tubes' chemical, electronic, and vibronic properties. Here, we compare the vibronic and electronic properties of pristine and partially oxidized CNTs using FT-IR and UV-Vis-NIR spectroscopy. In addition, we present a detailed comparison of individual thin bundles of unmodified and oxidized SWCNTs, based upon a combination of AFM and confocal scanning Raman microscopy.

EXPERIMENTS AND RESULTS

The SWCNTs, produced by the arc discharge method, were purchased from CarboLex (Lexington, KY). The unmodified tubes were dispersed by ultrasonic treatment in aqueous surfactant solution (1 wt% lithium dodecylsulfate) and centrifuged for 30 min at 8,000 rpm. The supernatant contains a clear solution of SWCNT bundles approximately 1–5 μm in length.[6] To oxidize the CNTs, 100 mg of the raw material was dispersed and refluxed in 150 mL nitric acid (65%) for three h.[7] Then the black solution was centrifuged and the remaining precipitate was washed with deionized water until the liquid phase showed a neutral pH. Before further processing, the oxidized SWCNTs were dried in vacuum for a few hours.

The first remarkable difference between the oxidized

*Author to whom correspondence should be addressed. E-mail: alf.mews@uni-mainz.de

and non-oxidized CNTs is their chemical behavior. Non-oxidized CNTs cannot be dissolved nor form a stable dispersion in any solvent investigated. However, with the aid of surfactant molecules, which form a micelle structure around the tubes, they can be dispersed in polar solvents such as water. The oxidized CNTs, on the other hand, are slightly soluble in, e.g., ethanol, even without the surfactant. This difference in solubility is explained by the increased polar nature of the tubes due to the formation of carboxylic and/or carbonyl functions on the tube or bundle surface.

The introduction of the oxygen-containing groups can be followed by IR spectroscopy. Figure 1 shows FT-IR spectra of non-oxidized and oxidized CNTs, both taken from KBr pellets in the wavelength range of typical vibrations of carbon–carbon and carbon–oxygen bonds. The following assignment of the absorption bands is based on IR studies of carbon surfaces which have been oxidized by different methods.[8] The bands in the region of 1380–1400 cm^{-1}, which appear in both the oxidized and non-oxidized sample, are ascribed either to carboxyl-carbonate structures or to aromatic C=C bonds and different substitution modes of the aromatic ring. The bands between 1580 and 1650 cm^{-1} are commonly attributed to C=C stretch vibrations. One indication of oxidation is the increased absorption at 1585 cm^{-1} for the oxidized tubes, which could be assigned to aromatic ring stretching coupled to highly conjugated carbonyl groups. However, the strongest signature of tube oxidation is the appearance of the additional band at 1725 cm^{-1}, as IR absorption bands in the region of 1860–1650 cm^{-1} are attributed to C=O stretch vibrations of carbonyl and carboxyl groups. In particular, absorption at 1724 cm^{-1}

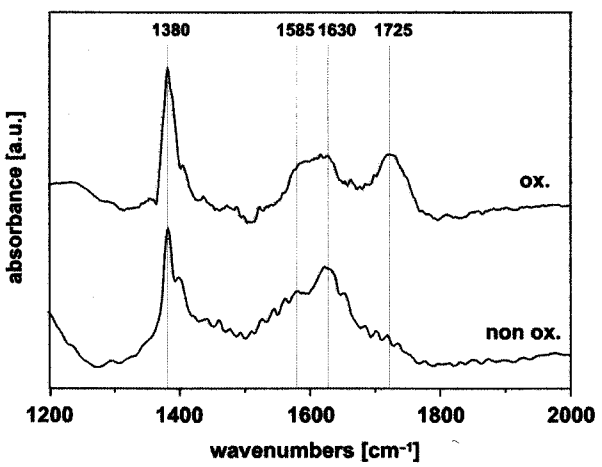

Fig. 1. FT-IR spectra of KBr pellets from oxidized (ox.) and non-oxidized (non ox.) carbon nanotubes. The oxidized tubes show an additional IR absorption at 1725 cm^{-1} attributed to C=O stretch vibrations.

was assigned to the presence of lactone groups, which were formed during the oxidation of carbon fibers. The same functional groups could also have been created during the oxidation process of the nanotubes.

Both the change in tube solubility and the appearance of additional bands in the IR spectrum after HNO_3 treatment provide evidence that the CNTs are oxidized, with oxygen-containing functional groups presumably formed at defects as reactive starting sites. It should be noted, however, that there might be an additional origin for the appearance of the carbonyl stretching vibration and the change in solubility. Since it has been shown that polycyclic aromatic hydrocarbons can be adsorbed on the nanotubes in high density, these (possibly oxidized) hydrocarbons might have been formed during the oxidation process and would represent a non-covalent side-wall functionalization.[9]

The question arises, to what extent the oxidation by HNO_3 changes the electronic properties of the tubes. Before discussing the possible changes of the electronic properties upon tube oxidation, we will briefly describe the classification and electronic properties of CNTs in general.[10]

CNTs can be viewed as a graphene sheet rolled up into a cylinder, and are classified according to their roll-up geometry described by the roll-up vector. The direction and length of this vector is defined in units of multiple integers (n,m) of the lattice vectors $(\mathbf{A_1},\mathbf{A_2})$ of the graphene sheet. From the structural point of view, CNTs can be divided into chiral and achiral tubes. Within the class of achiral CNTs, which are characterized by a roll-up vector along a high symmetry axis of the graphene sheet, there exist zig-zag tubes with $m = 0$, and armchair tubes with equal indices $(n = m)$. In general, CNTs are metallic if $|n-m| = 3q$, where q is an integer, or are semiconducting in any other case. The electronic structures of semiconducting and metallic CNTs are compared in Fig. 2. Both type of tubes show van Hove singularities as spikes in their density of states (DOS), each corresponding to a single quantum subband. The metallic CNTs possess a finite DOS at the Fermi level, whereas the semiconducting tubes show a band gap. The energy separation of those electronic singularities can be measured, for example, by optical absorption spectroscopy,[11] with the spectral position of the optical transitions depending on the tube diameter.

In order to study the effect of oxidation on the electronic properties of CNTs, we acquired UV-Vis-NIR absorption spectra of the oxidized and non-oxidized tubes. Absorption spectra in the UV-Vis were obtained from dispersions of the CNTs in a suitable solvent such as ethanol or water. For absorption measurements up to 2500 nm, where solvent absorption will interfere, the

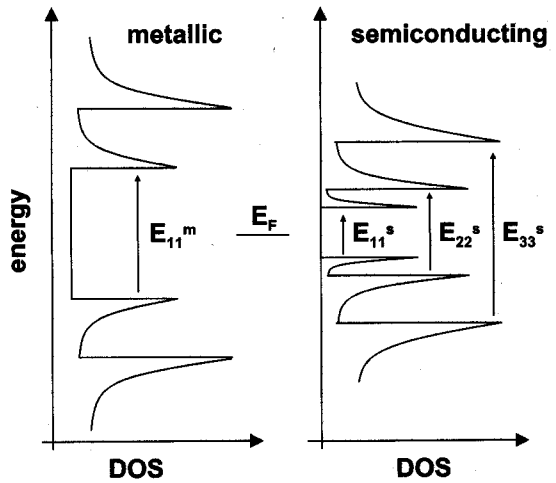

Fig. 2. Electronic structures of metallic and semiconducting CNTs. Optical transitions are allowed between mirror-like singularities, which appear as spikes in the density of states (DOS) in both types of tubes. The semiconducting tubes show a finite band gap, whereas the metallic tubes have a non-zero DOS at the Fermi level E_F.

tubes were deposited on a solid support. For that purpose, a dispersion of CNTs was sprayed onto a thin cover slip, which was heated to a temperature of ~150 °C to ensure fast solvent evaporation. Optical absorption measurements were performed with a Bruins Instruments (Puchheim, Germany) Omega 10 spectrometer operating in a wavelength range of 300–2500 nm.

The absorption spectra of oxidized and non-oxidized CNTs on solid support are presented in Fig. 3a. In general, optical spectra of CNTs show a featureless absorption, which increases towards higher energies, superimposed by absorption bands. The increasing absorption towards shorter wavelengths is attributed to plasmon excitation due to the collective motion of the conjugated π-electrons of the CNTs,[12] and is partly due to light scattering of the slightly turbid substrate. The superimposed absorption bands are related to resonant transitions between the electronic singularities of the CNTs, and are recognized in the inset of Fig. 3a where the π-plasmon background was subtracted for clarity. Comparing these absorption spectra with the electronic level structure in Fig. 2, it is clear that absorption bands I, II, and IV are due to resonant transitions of semiconducting CNTs, whereas absorption band III results from the metallic CNTs. The width of the absorption bands largely results from different metallic and semiconducting CNTs within the inhomogeneous sample. Better-resolved bands can be obtained by taking solution spectra (displayed in Fig. 3b) within the energy range of 1.1–3.1 eV. The three groups of bands in those spectra can be attributed to the second electronic transition of semiconducting tubes (E_{22}^s) in the energy range of 1–1.5 eV,

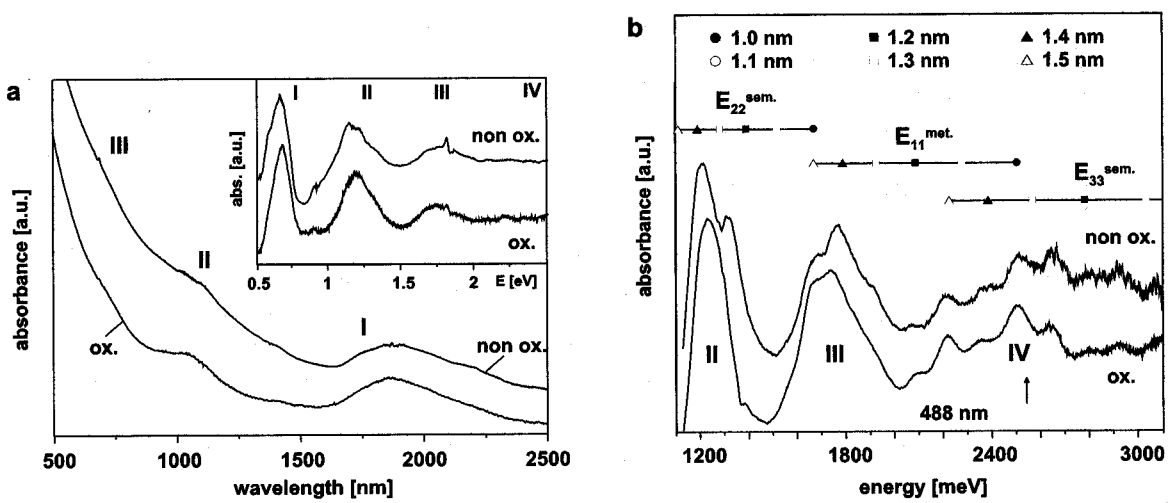

Fig. 3. UV-Vis-NIR absorption spectra of oxidized (ox.) and non-oxidized (non ox.) CNTs on a solid support (a), and in solution (b). a: The increasing absorption towards shorter wavelengths is due mainly to π-plasmons, whereas the superimposed structure results from resonant excitation between the electronic singularities. The inset shows the spectra after subtracting the background. Absorption features labeled I, II, and IV correspond to the electronic transitions E_{11}^s, E_{22}^s, E_{33}^s of the semiconducting tubes respectively; the absorption band labeled III stems from the transition E_{11}^m of the metallic tubes. b: The spectra of the oxidized tubes dispersed in ethanol and of the non-oxidized tubes in water show more clearly the optical transitions in the energy range above 2 eV after background subtraction. The absolute intensity of these absorption features is only of the order of a few percent of the original OD. In addition, the energetic positions calculated for an arbitrary series of metallic and semiconducting tubes are plotted for comparison (symbols).

the first transition of metallic tubes (E_{11}^m) between 1.5 and 2 eV, and the third resonant transition of semiconducting CNTs above 2 eV (E_{33}^s). To highlight the sensitive dependence of the optical transition energies upon the SWCNT diameter, we include in Fig. 3b the transition energies expected for an arbitrary series of different semiconducting and metallic tubes in the diameter range of 1–1.5 nm. These values were calculated according to Charlier and Lambin[13] using the following approximations:

$$E_{22}^s(d) = 4a_{c-c}\gamma_0 / d$$

$$E_{23}^s(d) = 8a_{c-c}\gamma_0 / d$$

$$E_{11}^m(d) = 6a_{c-c}\gamma_0 / d$$

In these formulas, d denotes the SWNT diameter, a_{C-C} is the nearest-neighbor carbon–carbon distance, taken as 1.44 Å, and γ_0 is the corresponding interaction energy for which a value of 2.9 eV is used.[14] It can be seen that a series of well-resolved optical transitions occurs in an energy range above 2 eV, most of which are attributed to the 3rd electronic transitions of the semiconducting CNTs (E_{33}^S). In the case of a large diameter distribution within the sample, some of those transitions might as well originate from thin metallic CNTs. For example, within the given model an optical transition at 2.2 eV might be associated with E_{11}^m for a metallic tube with d ~1.1 nm, or to E_{33}^s for a semiconducting tube with d = 1.5 nm. From the position and the width of the optical transitions, it can be estimated that the investigated tubes have a diameter between 1.1 and 1.5 nm, based on the theory referred to above. A detailed calculation of the diameter distribution based on the absorption measurements is difficult because different tubes could have different oscillator strengths. However, in our experiments, the absorption strength of the oxidized and non-oxidized samples cannot be compared directly because the sprayed films (as well as the NT suspensions) do not contain exactly the same amount of non-oxidized or oxidized material.

A second effect of the tube oxidation, besides a change in absorption strength, might be an energetic shift of the electronic levels, which would most likely result in a shift of the absorption bands. In our samples, there was no detectable shift of any of the resolved transitions after CNT oxidation, especially in the energy range above 2 eV, which is important for the Raman spectroscopy (see below).

So far, we have compared spectroscopic ensemble measurements of the vibrational and electronic properties of oxidized and non-oxidized CNTs. We now present resonance-enhanced Raman studies on single tubes (thin bundles). In particular, we focus on the laterally resolved investigation of individual oxidized and non-oxidized CNT (bundles) by both atomic force microscopy (AFM) and Raman microscopy. Extending our recent investigations of individual, unmodified CNT bundles using these techniques and special substrates with appropriate markers,[15] we compare the tube or bundle thickness and their Raman activity before and after oxidation of the CNTs.

A Raman image of well-separated, non-oxidized CNTs is displayed in Fig. 4 (right). For sample preparation, the tubes were adsorbed from dispersion on a Suprasil quartz surface modified with (3-aminopropyl)-triethoxysilane (0.1% in water, 2 min), for 30 min. Subsequently, the sample was rinsed with water, blown dry, and placed in a confocal Raman microscope. The microscope set-up is based on an inverted Zeiss microscope equipped with a piezo scanner and a high numerical aperture microscope objective (NA = 0.9).[16] For excitation, 1 mW of circular polarized light (λ_{exc} = 488 nm) was focused on a nearly diffraction limited spot size (∅ 300 nm), resulting in an excitation intensity of ~1 MW/cm^2 in the center of the excitation spot. The sample was raster scanned through the excitation spot and the back scattered light was collected with the same microscope objective. After passing a holographic notch filter, the light was guided to a photon counting module and/or to a spectrograph equipped with a liquid nitrogen-cooled CCD camera. A spectrum of unmodified CNTs, recorded during one scan, is shown in Fig. 4 (left). The peak at 488 nm originates from residual light of the excitation laser, whereas the band around 529 nm, shifted by 1590 cm^{-1} from the excitation line, is due to the Raman signal of the CNTs. The Raman image reflecting the G-lines of the nanotubes (Fig. 4, right) clearly demonstrates that individual CNTs can be located and investigated by their strong Raman signal in an optical microscope even on a simple glass substrate.

In order to directly compare the Raman signal of oxidized and non-oxidized CNTs, it is important to investigate the different tubes next to each other within the same experiment because slight differences in the experimental setup (e.g., slight defocusing) will lead to differences in the Raman intensities detected. Also, it is necessary to locate the same tubes and investigate their geometry with an AFM microscope since Raman intensity scales with bundle thickness. To meet these requirements, we used a substrate with lithographically defined electrode structures suitable as markers, enabling us to address the same sample area in the AFM, as well as the Raman microscope. This substrate consists of a 15-nm-thick Si_3N_4 membrane, which is transparent for the laser light and has a sufficiently low surface roughness to allow for a detailed AFM investigation.[17] First, only

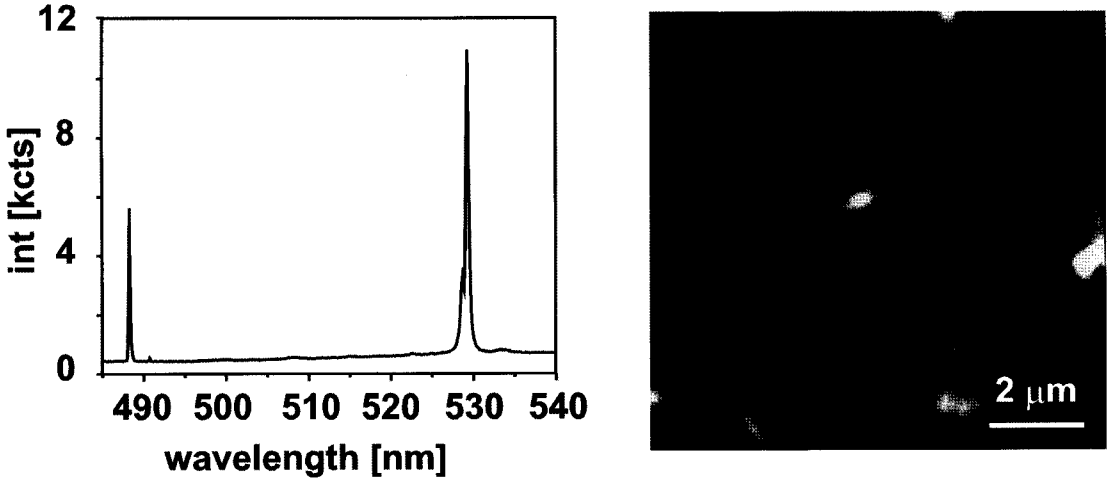

Fig. 4. Raman imaging of individual, unmodified CNTs deposited on a quartz substrate. The left spectrum is taken while the sample is scanned through the excitation spot of a confocal microscope. The spectrum consists of remaining scatter and Rayleigh light of the laser at 488 nm, as well as the Raman G-line of CNTs around 528 nm. To the right is a Raman image (512*512 pixels) based upon the G-line of the tubes excited with ~1 MW/cm^2 in the center of the excitation spot.

non-oxidized CNTs were deposited, and their position was determined with an AFM microscope, as can be seen in Fig. 5a. Then we deposited only oxidized CNTs on the same substrate, allowing us to distinguish between the chemically different tubes via AFM inspection. The AFM image of the substrate after this second deposition is presented in Fig. 5b. In Fig. 5c, we display both the thickness, derived from the AFM section profile, and the Raman intensity taken from the Raman image (not shown) of the single non-oxidized CNT bundle marked in Fig. 5a. As for the Raman imaging, only the intensity of the G-lines is spectrally selected with a monochromator; the Raman intensities in Fig. 5c and 5d are directly proportional to the G-line intensities at different positions. The values of the Raman intensity and AFM height were determined from line scans perpendicular to the tube axis and subtracting a linear background at each point.

It is apparent from the AFM height profile in Fig. 5c that this particular non-oxidized bundle is not uniformly thick. The lower part of the bundle, which sticks to the electrode, has a thickness of 2–3 nm and therefore consists of approximately 4–6 single CNTs. Towards the bundle end within the upper half of the image, the bundle becomes considerably thinner with a height of the order of 1 nm, which is attributed to a single CNT sticking out of the bundle. This tube can still be identified by its Raman signal, with a count rate of approximately 500 cts/s in the present experiment. In Fig. 5e, Raman spectra taken at four different positions (I, II, III, IV) along this specific bundle are displayed. For clarity, the spectra were normalized to the same height (the absolute Raman intensity can be seen from the intensity profile in Fig. 5c). Considering that the CNTs investigated evolve from a bundle into a single tube, spectra I and II belong to the bundle section, whereas spectra III and IV originate from the single SWNT. A closer inspection of the spectra reveals a slight shift of the peak center position from 1591.6 cm^{-1} for spectrum No. I to 1593.5 cm^{-1} for spectrum No. IV, and that the spectral width narrows from 9.7 cm^{-1} down to 6.9 cm^{-1} as fitted by single Lorenzians. As the spectral resolution of our setup is 2 cm^{-1}, we assume that the homogeneous G-line width of a single SWCNT is ~5 cm^{-1}.

Figure 5d shows a comparison of the Raman intensity profile and the bundle height taken from the oxidized bundle that is marked in Fig. 5b. This particular bundle is identified as an oxidized CNT bundle, which was deposited during the second deposition. Comparison of the Raman intensity and AFM height profiles of the oxidized CNTs in Fig. 5d with those of the non-oxidized CNTs in Fig. 5c reveals that the Raman activity is strongly reduced after oxidation. The oxidized bundle is about 6–7 nm in height and yields a maximum Raman signal of about 700 cts/s, whereas the non-oxidized bundle of 4–5 nm in height yields approximately 1500 cts/s. Figure 5f shows different spectra of the oxidized tube bundle at positions (V, VI, VII, VIII) labeled in Fig. 5b. The somewhat noisy appearance of the normalized spectra results from the decreased S/N ratio after oxidation. A fitting procedure clearly revealed almost identical band positions as compared to the spectra

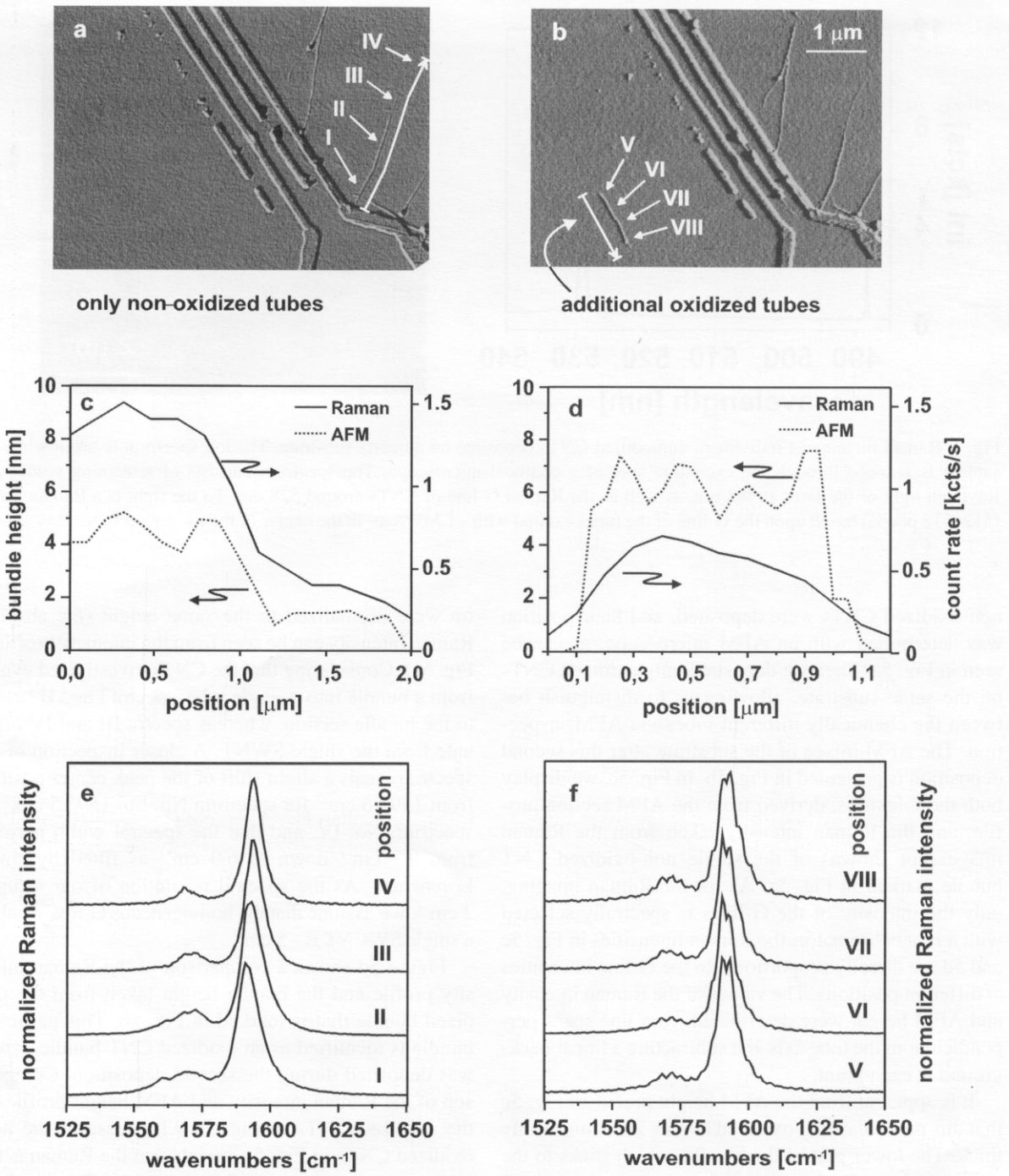

Fig. 5. Correlation of Raman and AFM data of single non-oxidized (a,c,e) and oxidized (b,d,f) CNT(bundles). 5a and 5b show AFM images of CNTs deposited on a Si_3N_4 membrane with electrode markers. Image (a) is taken after deposition of non-oxidized CNTs, and image (b) shows the same sample area after adding oxidized CNTs. 5c and 5d show both a Raman and an AFM line scan along a single non-oxidized and oxidized tube bundle, respectively. The non-oxidized bundle in 5c is not uniformly thick but eventually evolves from a bundle into a single tube. The oxidized bundle in 5d is much thicker than the non-oxidized bundle in 5c, but yields less Raman photons under the same experimental conditions. 5e and 5f show spectra taken at different positions along the tube. The spectra in 5e show that there are slightly different peak centers and that the spectral width narrows down from 10 to 7 cm^{-1} when the bundle becomes thinner. The spectra of the oxidized tubes in 5f show that the spectral position of the G-line does not change significantly upon tube oxidation.

of the non-oxidized tubes in Fig. 5e. For example, spectrum V has a center of the G-line at 1592.2 cm^{-1} (FWHM: 8.3 cm^{-1}), whereas the center of spectrum No. VIII is found at 1591.8 cm^{-1} (FWHM: 10 cm^{-1}).

DISCUSSION

Resonance-enhanced Raman spectroscopy is a useful tool to gain information about both the vibronic and the electronic properties of CNTs.[18] In our experiments, no significant change of the G-line position was observed after oxidation of the tubes. On the other hand, Yu and Brus reported broadening of Raman scattering, which they attributed to charge transfer due to chemical doping.[19] However, it is important to note that Yu and Brus used excitation at 632 nm, for which Raman scattering from metallic tubes is the dominant contribution. In the present report, in contrast, the laser wavelength of 488 nm is expected to predominantly excite the semiconducting tubes.

The decrease of the Raman intensity observed for the oxidized tubes could be due to a change in the electronic properties and/or an alteration of the vibrational modes of the tubes. Oxidation might shift the electronic transitions out of resonance, for example, due to a change in the tube diameter distribution, or decrease the absorption cross section (oscillator strength) of the tubes, both of which would decrease the resonant Raman cross section. Considering the first possibility, Fig. 3 does not reveal a pronounced shift of the well-resolved absorption bands in the region of the excitation wavelength (λ_{exc} = 488 nm). Although the width of those absorption bands is quite broad (>100 meV), we conclude that the oxidation procedure used in our experiments does not cause changes in the absorption energies that can significantly reduce the resonant enhancement in the Raman process. Further studies, however, would be helpful to independently prove that the tube diameter is not affected by the oxidation procedure. This goal could be achieved by investigating the radial breathing mode in the Raman spectra. It should be noted again that possible differences in the absorption coefficients, which might arise because the oxidation process could influence the electronic density of states, cannot be extracted from the absorption data in Fig. 3. Therefore, we cannot exclude the possibility that such an effect could lead to different resonance enhancement conditions.

In light of the above considerations, we attribute the decrease of the Raman intensity predominantly to changes in the local bonding geometry. The newly formed chemical groups incorporating oxygen atoms, although most likely not detectable by Raman spectroscopy of single tubes, may influence the symmetry of the tubes and hence affect the quantum mechanical selection rules. It also might influence the coherence of the phonons, because the fact that individual CNTs can be investigated by Raman microscopy is mainly due to thousands of atoms vibrating in phase, leading to an effective Raman cross section of the order of 10^{-21} cm^2.[15] Detailed calculations are required to clarify the quantum mechanical nature of the intensity decrease. Here we can only speculate about the degree of the oxidation process and possible oxidation sites: In a first scenario, it might well be that only the CNTs in the periphery of a given bundle are oxidized, while the tubes in the bundle interior remain unaffected. In the second scenario, all tubes within a given bundle are chemically modified to the same degree. In order to distinguish between these two cases, we plotted (Fig. 6) the Raman-G-line intensity as a function of bundle height for a number of representative oxidized and non-oxidized CNT bundles. The two plots clearly show that there is a square dependence of the Raman intensity upon bundle height as a result of the "on average" quadratic geometry of the bundle cross section. The plots vary by a factor of 4, i.e., the Raman activity of the non-oxidized tubes is on average 4 times higher for all the tubes within a given bundle. It is of importance that even the thinnest oxidized bundle, which is probably a single oxidized tube as judged from its height, still yields a detectable Raman signal. Therefore, we assume that all tubes within a given bundle are oxidized to the same degree.

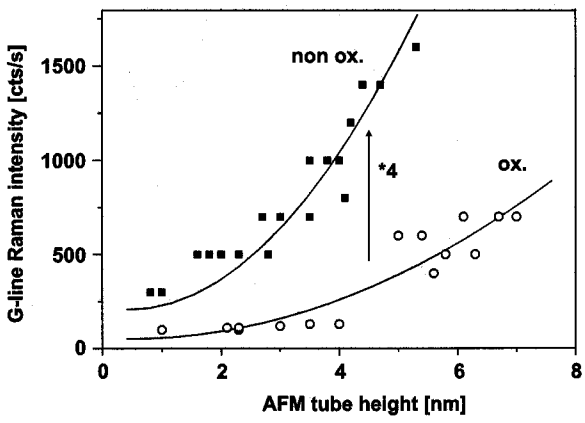

Fig. 6. Comparison of the G-line intensity of non-oxidized (non ox.) and oxidized (ox.) CNT bundles. The solid lines were drawn to highlight the quadratic dependence of the Raman intensity upon tube height, which results from the geometry of the bundle cross section. The non-oxidized CNTs yield on average 4 times more Raman photons under the same experimental conditions than the oxidized CNTs.

CONCLUSION

A detailed spectroscopic study of partially oxidized CNTs was presented. Tube oxidation followed by FTIR spectroscopy revealed an additional absorption band of the C=O stretch vibration after the treatment of CNTs in HNO_3 solution. NIR-UV-Vis absorption measurements did not reveal any significant shift of the electronic transitions upon tube oxidation. Individual oxidized and non-oxidized CNT (bundles) were investigated by confocal scanning resonance Raman microscopy. The G-line shape and position of semiconducting CNTs were found to be almost unaffected by oxidation. In addition, the combination with AFM microscopy allowed for a detailed comparison of the bundle geometry and Raman intensity of the same tubes. The Raman intensity of the oxidized CNTs was observed to be reduced by a factor of ~4 compared to pristine tubes. As the bulk UV-Vis spectra did not show pronounced changes in the electronic structure of the tubes, we attribute the intensity decrease to a change in the tubes vibronic structure leading to different phonon modes/densities.

Acknowledgments. The authors thank Prof. Manfred Kappes for stimulating discussions. This work was supported by the Bildungsministerium für Bildung und Forschung (BMBF) under contract No. 03C0302B9.

REFERENCES AND NOTES

(1) Dalton, A.B.; Stephan, C.; Coleman, J.N.; McCarthy, B.; Ajayan, P.M.; Lefrant, S.; Bernier, P.; Blau, W.; Byrne, H.J. *J. Phys. Chem. B* **2000**, *104*, 10012–10016.

(2) Chen, J.; Hamon, M.A.; Hu, H.; Chen, Y.; Rao, A.M.; Eklund, P.C.; Haddon, R.C. *Science* **1998**, *282*, 95–98.

(3) Mickelson, E.T.; Huffman, C.B.; Rinzler, A.G.; Smalley, R.E.; Hauge, R.H.; Margrave, J.L. *Chem. Phys. Lett.* **1998**, *296*, 188–194.

(4) Boul, P.J.; Liu, J.; Mickelson, E.T.; Huffman, C.B.; Ericson, L.M.; Chiang, I.W.; Smith, K.A.; Colbert, D.T.; Hauge, R.H.; Margrave, J.L. *Chem. Phys. Lett.* **1999**, *310*, 367–372.

(5) Holzinger, M.; Hirsch, A.; Bernier, P.; Duesberg, G.S.; Burghard, M. In *Electronic Properties of Novel Materials—Molecular Nanostructures*; Kuzmany, K.H.; Fink, J.; Mehring, M.; Roth, S., Eds.; Proc. No. 544, American Institute of Physics, New York, 2000; pp 246–249.

(6) Duesberg, G.S.; Muster, J.; Byrne, H.J.; Roth, S.; Burghard, M. *Appl. Phys. A* **1999**, *69*, 269–274.

(7) Burghard, M.; Krstic, V.; Duesberg, G.S.; Philipp, G.; Muster, J.; Roth, S.; Journet, C.; Bernier, P. *Synth. Met.* **1999**, *103*, 1540–1542.

(8) Moreno-Castilla, C.; López-Ramón, M.V.; Carrasco-Marín, F. *Carbon* **2000**, *38*, 1995–2001 and references therein.

(9) Chen, R.J.; Zhang, Y.; Wang, D.; Dai, H. *J. Am. Chem. Soc.* **2001**, *123*, 3838–3839.

(10) Saito, R.; Dresselhaus, G.; Dresselhaus, M.S. *Physical Properties of Carbon Nanotubes*, Imperial College Press: London, 1998.

(11) Chiang, I.W.; Brinson, B.E.; Smalley, R.E.; Margrave, J.L.; Hauge, R.H. *J. Phys. Chem. B* **2001**, *105*, 1157–1161.

(12) Yu, Z.; Brus, L. *J. Phys. Chem. B* **2001**, *105*, 1123–1134.

(13) Charlier, J.C.; Lambin, P. *Phys. Rev. B* **1998**, *57*, R15037-R15039.

(14) Brown, S.D.M.; Corio, P.; Marucci, A.; Dresselhaus, M.S.; Pimenta, M.A.; Kneipp, K. *Phys. Rev. B* **2000**, 61, R5137–R5140.

(15) Mews, A.; Koberling, F.; Basche, T.; Philipp, G.; Duesberg, G.S.; Roth, S.; Burghard, M. *Adv. Mater.* **2000**, *12*, 1210–1214.

(16) Koberling, F.; Mews, A.; Basché, T. *Adv. Mater.* **2001**, *13*, 672–676.

(17) Philipp, G.; Burghard, M.; Duesberg, G.S.; Roth, S.; Klitzing, K. v. In *Electronic Properties of Novel Materials—Progress in Molecular Nanostructures*; Kuzmany, K.H.; Fink, J.; Mehring, M.; Roth, S., Eds.; Proc. No. 442, American Institute of Physics, New York, 1998; pp 74–78.

(18) Dresselhaus, M.S.; Eklund, P.C. *Adv. Phys.* **2000**, *49*, 705–814.

(19) Yu, Z.; Brus, L.E. *J. Phys. Chem. A* **2000**, *104*, 10995–10999.